AIP | Journal of Applied Physics

Thermoelectric properties of p-type (Bi2Te3) x (Sb2Te3)1−x single crystals doped with 3wt. % Te

Ö. Ceyda Yelgel and G. P. Srivastava

Citation: Journal of Applied Physics **113**, 073709 (2013); doi: 10.1063/1.4792653
View online: http://dx.doi.org/10.1063/1.4792653
View Table of Contents: http://scitation.aip.org/content/aip/journal/jap/113/7?ver=pdfcov
Published by the AIP Publishing

Thermoelectric properties of p-type $(Bi_2Te_3)_x(Sb_2Te_3)_{1-x}$ single crystals doped with 3 wt. % Te

Ö. Ceyda Yelgel and G. P. Srivastava
School of Physics, University of Exeter, Stocker Road, Exeter EX4 4QL, United Kingdom

(Received 3 January 2013; accepted 4 February 2013; published online 20 February 2013)

In the present work, thermoelectric properties of p-type $(Bi_2Te_3)_x$ $(Sb_2Te_3)_{1-x}$ single crystals doped with 3 wt. % Te are theoretically explored for various chemical compositions ($x = 0.18$, 0.19, 0.20, 0.22, 0.24, 0.26) in the temperature range of 290–500 K. The influence of the chemical composition in enhancing the thermoelectric figure of merit (ZT) is discussed in detail. Using the nearly-free electron approximation and the Fermi-Dirac statistics, the temperature dependences of Fermi level (E_f), Seebeck coefficient (S), and electrical conductivity (σ) are successfully reproduced as reported in the experimental study of Li *et al.* [Intermetallics **19**, 2002 (2011)]. The thermal conductivity contributions from phonons (κ_{ph}), acceptor holes (κ_h), and electron-hole pairs (κ_{bp}) are included by employing Srivastava's scheme, Wiedemann-Franz law, and Price's theory, respectively. By combining all three contributions of the thermal conductivity we successfully explain the experimental measurements of the total thermal conductivity as reported by Li *et al.* Furthermore, it is theoretically found that among all the compositions the p-type 20%(Bi_2Te_3)-80%(Sb_2Te_3) sample has the maximum ZT value of 1.31 at 390 K, which is also in good agreement with the experimental results obtained by Li *et al.* © *2013 American Institute of Physics*. [http://dx.doi.org/10.1063/1.4792653]

I. INTRODUCTION

Thermoelectric (TE) devices can generate electric voltage from temperature differences and *vice versa*. TE materials are becoming one of the most important solutions for today's energy challenges. They have a wide range of applicability in power generation and solid-state cooling.[1–5] The TE device utility is directly evaluated via the dimensionless thermoelectric figure of merit quantity (ZT) expressed as

$$ZT = \frac{\sigma S^2}{\kappa_c + \kappa_{ph} + \kappa_{bp}} T, \quad (1)$$

where T is the absolute temperature, S is the Seebeck coefficient, σ is the electrical conductivity, and κ_c, κ_{ph}, κ_{bp} are the carrier (electron or hole), phonon (lattice), and electron-hole pairs (bipolar) contributions of the thermal conductivity, respectively.[1–5] Efficient and competitive TE materials require high values of ZT, requiring special attention to strong interrelation between all three transport coefficients (S, σ, and $\kappa_c + \kappa_{ph} + \kappa_{bp}$). By getting the maximised power factor ($S^2\sigma$) and/or the minimised total thermal conductivity (κ_{total}) the efficiency of TE materials can be improved.[1–3,6–8] Numerous investigations show that the most dominant factor to have an enhanced value of ZT is reduced lattice thermal conductivity.[6–9] There are several ways to minimise κ_{ph}, such as making alloys, varying chemical compositions, and using low-dimensional systems.[6–9] Recent studies have indicated that ZT could be significantly improved by using low dimensional systems with large phonon scattering rate.[9–15] By adopting this approach extraordinarily large values of ZT were claimed experimentally for p-type Bi_2Te_3/Sb_2Te_3 superlattices as 2.4 at room temperature[12] and PbSeTe/PbTe quantum dot superlattices as 3.0 at 550 K.[16]

Among various TE materials, Bi_2Te_3 based alloys (both n-type and p-type) are the most widely used materials due to their usefulness in the room temperature range and capability to enhance their ZT values ($ZT > 1$) by diverse methods.[1,8,17] There are so many experimental studies on thermoelectric properties of Bi_2Te_3 based materials, for instance, crystals,[18,19] thin-films,[12,20] and nanowires.[21] These materials have rhombohedral structure with the space group $R\bar{3}m$ and for Bi_2Te_3 five atomic layers stack along the c axis by van der Waals interactions in the sequence Te^1-Bi-Te^2-Bi-Te^1.

In this present study, we report a detailed theoretical investigation of the thermoelectric coefficients (E_f, S, σ, κ_{total}, ZT) of p-type $(Bi_2Te_3)_x(Sb_2Te_3)_{1-x}$ single crystals in the composition range of $0.18 \leq x \leq 0.26$ and compare our results with the experimental results obtained by Li *et al.*, whose samples were prepared by the fusion method together with spark plasma sintering.[22] Moreover, a theoretical discussion is presented to clarify the significant influence of the chemical composition on ZT. In agreement with the experimental work[22] it is theoretically found that ZT can be improved up to 1.31 at 390 K by taking $x = 0.20$. Temperature dependence of E_f for both extrinsic and intrinsic regimes is calculated following our previously reported work.[23] The Hicks-Dresselhaus theory is applied for the calculation of the temperature dependence of S, σ, and κ_c.[9] The temperature variation of κ_{ph} is worked out by Srivastava's scheme[24] rigorously. The Price's theory[25] is applied for the temperature dependent calculation of κ_{bp}.

II. THEORY

A. Electronic transport coefficients

The electronic transport coefficients of thermoelectric semiconductor materials (S, σ, and κ_c) strongly depend on

temperature dependent Fermi level. In p-type semiconductors, in the extrinsic regime, the temperature variation of E_f is expressed as[26]

$$E_f^{ext} = \frac{1}{2}(E_a + E_v) + \frac{k_B T}{2}\ln\frac{N_a}{2U_v} - k_B T \sinh^{-1}\left(\sqrt{\frac{U_v}{8N_a}}\exp\left(\frac{-\Delta E_i}{2k_B T}\right)\right), \quad (2)$$

where E_v is the valence band edge, E_a is the acceptor energy level, N_a is the concentration of acceptor impurity atoms, $\Delta E_i = E_a - E_v$ is the acceptor ionisation energy, and $U_v = 2((m_p^* k_B T)/(2\pi\hbar^2))^{3/2}$ with m_p^* as the hole effective mass, k_B is the Boltzmann constant, and $\hbar$ is the reduced Planck's constant. The Fermi level at zero temperature, $E_f = (E_v + E_a)/2$, lies exactly midway between the acceptor level and the valence band. As the temperature increases, the Fermi level first decreases slowly and then increases until it reaches the value where the acceptor level becomes fully ionized.[26] Thus, from this point the material behaves like an intrinsic semiconductor and the temperature dependence of E_f is expressed as[26]

$$E_f^{int} = \frac{E_v + E_c}{2} + \frac{3}{4}k_B T \ln\left(\frac{m_p^*}{m_n^*}\right), \quad (3)$$

where E_c is the conduction band edge and m_n^* is the electron effective mass.

In p-type semiconductors, the Seebeck coefficient S is expressed within a single-band nearly free-hole model as[9]

$$S = \frac{k_B}{e}(\delta - \zeta^*), \quad (4)$$

where e is the hole charge and $\zeta^* = E_f/k_B T$ is the reduced chemical potential. The δ function in Eq. (4) is described as[4,27]

$$\delta = \frac{(r+\frac{5}{2})F_{r+\frac{3}{2}}(\zeta^*)}{(r+\frac{3}{2})F_{r+\frac{1}{2}}(\zeta^*)}, \quad (5)$$

where r is a scattering parameter and F_i is the Fermi integral given by[9]

$$F_i = \int_0^\infty \frac{x^i dx}{e^{(x-\zeta^*)}+1}. \quad (6)$$

The general expression for the electrical conductivity of semiconductors is

$$\sigma = ne\mu_c = n\frac{e^2}{m_c^*}\langle\tau\rangle, \quad (7)$$

where μ_c is the carrier conductivity mobility, m_c^* is the conductivity effective mass (taken as m_p^* for p-type material), $\langle\tau\rangle$ is the average relaxation time of carriers, and n is the carrier concentration (taken as N_a for p-type material).[27,28] We can express Eq. (7) in the extrinsic and intrinsic limits. In the extrinsic regime the electrical conductivity is expressed as[23]

$$\sigma_{ext} = \frac{4}{3\pi\sqrt{\pi}}\frac{e^2}{m_c^*}\frac{\hbar\rho c_L^2}{E_D^2}F_{1/2}, \quad (8)$$

with the assumption that the hole-acoustic phonon scattering mechanism is the most dominant mechanism. In Eq. (8), c_L is the velocity of longitudinal phonons, ρ is the mass density, and E_D is the deformation potential. By following Wilson's expression[29] the electrical conductivity in the intrinsic regime is given by

$$\sigma_{int} = A' e^{-E_g/2k_B T}, \quad (9)$$

where A' can be taken as a temperature independent parameter.

B. Thermal transport coefficients

The carrier contribution (namely holes in the present work) to the thermal conductivity can be expressed by following the Wiedemann-Franz law:[27]

$$\kappa_c = \sigma\mathcal{L}T = \left(\frac{k_B}{e}\right)^2 \sigma T\mathcal{L}_0, \quad (10)$$

where $\mathcal{L}$ is the Lorenz number and for semiconductors $\mathcal{L}_0$ can be described in terms of the scattering parameter r and the Fermi integral[4,27]

$$\mathcal{L}_0 = \frac{(r+\frac{7}{2})F_{r+\frac{5}{2}}(\zeta^*)}{(r+\frac{3}{2})F_{r+\frac{1}{2}}(\zeta^*)} - \left[\frac{(r+\frac{5}{2})F_{r+\frac{3}{2}}(\zeta^*)}{(r+\frac{3}{2})F_{r+\frac{1}{2}}(\zeta^*)}\right]^2. \quad (11)$$

The bipolar contribution (electron-hole pairs) to the thermal conductivity (κ_{bp}) becomes significant above room temperature in narrow band-gap semiconductors.[25,30] This contribution can be expressed as

$$\kappa_{bp} = F_{bp} T^p \exp(-E_g/2k_B T), \quad (12)$$

with F_{bp} and p regarded as adjustable parameters depending on doping type.[23]

The lattice contribution to the thermal conductivity is investigated by employing Debye's isotropic continuum model within the single-mode relaxation time approximation[24]

$$\kappa_{ph} = \frac{\hbar^2 q_D^5}{6\pi^2 k_B T^2}\sum_s c_s^4 \int_0^1 dx x^4 \tau\bar{n}(\bar{n}+1), \quad (13)$$

where τ is the phonon relaxation time, q_D is the Debye radius, $x = q/q_D$ is a reduced wavenumber, s represents the polarisation branch of phonon (longitudinal or transverse), $\bar{n}$ is the Bose-Einstein distribution function, and c_s is the velocity of phonons for polarisation branch s.

The phonon relaxation rate τ^{-1} in Eq. (13) is contributed by several scattering mechanisms: boundary (bs), mass defects (md), carriers (hp), and anharmonic (anh). Using the Matthiessen rule we can write $\tau^{-1} = \sum_i \tau_i^{-1}$, where τ_i^{-1} represents the contribution from i^{th} scattering mechanism.[24] The

scattering of phonons with the boundaries of a sample is defined as

$$\tau_{qs}^{-1}(bs) = \frac{c_s}{L}, \tag{14}$$

with the phonon mean free path determined by crystal size as L.[24,31] The mass defect scattering of phonons in semiconductor alloys arises from two different sources: isotopes and the effect of alloying. The scattering of phonons from both types of mass defects can be expressed in the form[24,32]

$$\tau_{qs}^{-1}(\mathrm{md}) = \frac{\Gamma_{\mathrm{md}}\Omega}{4\pi\bar{c}^3}\omega^4(qs), \tag{15}$$

where Ω is the volume of a unit cell, $\bar{c}$ is the average phonon velocity, and $\omega = cq$. Expressions for the isotopic and alloying contributions towards Γ_{md}, viz. $\Gamma_{\mathrm{isotopes}}$ and Γ_{alloy}, are given in our previous publication.[23] The scattering rate of longitudinal phonons of frequency ω by acceptor holes can be written as[33]

$$\tau_{ql}^{-1}(\mathrm{hp}) = \frac{N_a E_D^2 \omega}{\rho c_L^2 k_B T}\sqrt{\frac{\pi m_p^* c_L^2}{2k_B T}}\exp\left(\frac{-m_p^* c_L^2}{2k_B T}\right). \tag{16}$$

While studying the phonon-phonon scattering mechanism we restrict ourselves to only three-phonon processes. We consider the three-phonon interaction using Srivastava's scheme[24]

$$\tau_{qs}^{-1}(\mathrm{anh}) = \frac{\hbar q_D^5 \gamma^2}{4\pi\rho\bar{c}^2}\sum_{s's''\varepsilon}\left[\int dx' x'^2 x''_+ [(1-\varepsilon+\varepsilon(Cx+Dx')] \times \frac{\bar{n}_{q's'}(\bar{n}''_+ + 1)}{(\bar{n}_{qs}+1)} + \frac{1}{2}\int dx' x'^2 x''_- [1-\varepsilon+\varepsilon(Cx-Dx')]\frac{\bar{n}_{q's'}\bar{n}''_-}{\bar{n}_{qs}}\right]. \tag{17}$$

Here γ is the Grüneisen constant, $x' = q'/q_D$, $x''_+ = Cx \pm Dx'$, $\bar{n}''_\pm = \bar{n}(x''_\pm)$, $C = c_s/c_{s''}$, $D = c_{s'}/c_{s''}$. $\varepsilon = 1$ for momentum-conserving normal processes, and $\varepsilon = -1$ for momentum-nonconserving Umklapp processes. The first and second terms in Eq. (17) are controlled by class 1 events $\boldsymbol{q}s + \boldsymbol{q}'s' \rightarrow \boldsymbol{q}''s''$ and class 2 events $\boldsymbol{q}s \rightarrow \boldsymbol{q}'s' + \boldsymbol{q}''s''$, respectively. The integration limits on the variables x and x' derived from a detailed consideration of the energy and momentum conservation requirements have been presented in Ref. 24. In the present study, the phonon-phonon scattering rate is treated by considering $F_{3\mathrm{ph}} = (\gamma/\bar{c})^2$ as an adjustable parameter, as we did in our previous works.[23,34]

III. RESULTS AND DISCUSSION

To investigate the thermoelectric properties of p-type $(Bi_2Te_3)_x(Sb_2Te_3)_{1-x}$ single crystals in the range $0.18 \leq x \leq 0.26$ we numerically evaluate all the integrals by using Simpson's rule. All the related parameters for the theoretical calculations are given in Table I.

TABLE I. Constants and parameters used in the calculations of thermoelectric properties of p-type $(Bi_2Te_3)_x$ $(Sb_2Te_3)_{1-x}$ single crystals doped with 3 wt. % Te.

Property/parameter	x = 0.18	x = 0.19	x = 0.20	x = 0.22	x = 0.24	x = 0.26
$E_g(0)$ (eV)	0.09	0.09	0.09	0.09	0.09	0.09
E_a (eV)	0.04	0.04	0.04	0.04	0.04	0.04
α (eV/K)	0.0105	0.0105	0.0105	0.0105	0.0105	0.0105
η (eV)	0.32	0.32	0.32	0.32	0.32	0.32
β (K)	14.53	14.53	14.53	14.53	14.53	14.53
N_a (m^{-3})	1.0×10^{25}	8.4×10^{24}	8.1×10^{24}	7.7×10^{24}	4.2×10^{24}	2.55×10^{24}
m_p^*/m_e^*	1.27	1.13	1.09	1.06	1.03	1.01
r	0.4	0.43	0.45	0.55	0.53	0.43
ρ (kg/m^3)[38]	6.67×10^3	6.68×10^3	6.69×10^3	6.72×10^3	6.75×10^3	6.77×10^3
$\bar{c}$ (m/s)[39]	2918.0	2920.3	2922.0	2925.4	2928.8	2932.2
a_{lat} (Å)[40]	4.27	4.27	4.28	4.28	4.28	4.28
E_D (eV)	32.0	32.0	32.0	32.0	32.0	32.0
ς	1.1	1.1	1.1	1.1	1.1	1.1
A ($K^{-1.1}$)	0.00063	0.00063	0.00058	0.00068	0.00064	0.0007
A' ($Ohm^{-1}\,m^{-1}$)	3.03×10^{-9}	3.03×10^{-9}	3.03×10^{-9}	3.03×10^{-9}	3.03×10^{-9}	3.03×10^{-9}
B ($Ohm\cdot m\cdot K^{-1}$)	2.8×10^{-8}	3.0×10^{-8}	3.1×10^{-8}	4.0×10^{-8}	4.7×10^{-8}	5.6×10^{-8}
p	1.0	1.0	1.0	1.0	1.0	1.0
F_{bp} ($W\,m^{-1}\,K^{-2}$)	13.0×10^{-4}	13.0×10^{-4}	13.0×10^{-4}	21.0×10^{-4}	35.0×10^{-4}	35.0×10^{-4}
q_D ($Å^{-1}$)	0.6	0.601	0.603	0.605	0.608	0.61
L (mm)	5.0	5.0	5.0	5.0	5.0	5.0
Ω ($Å^3$)	160.2	160.3	160.414	160.6	161.0	161.0
$\Gamma_{\mathrm{isotopes}}$	0.028	0.026	0.025	0.0078	0.0054	0.00186
Γ_{alloy}	0.053	0.051	0.05	0.016	0.011	0.004
$F_{3\mathrm{ph}}$ (s^2/m^2)	1.06×10^{-5}	1.058×10^{-5}	1.057×10^{-5}	1.055×10^{-5}	1.052×10^{-5}	1.05×10^{-5}

A. Electronic transport coefficients

The theoretical result for the Fermi level variation with temperature for p-type $(Bi_2Te_3)_x(Sb_2Te_3)_{1-x}$ single crystals is presented in Fig. 1. All samples exhibit a change from the extrinsic to the intrinsic behaviour above room temperature. This behaviour is entirely supported by the experimental Seebeck coefficient measurements reported in reference.[22] For all the six compositions, E_f first falls smoothly in the extrinsic regime and then rises up linearly in the intrinsic regime. In narrow band gap semiconductors, band gap variation with temperature plays a major role in the intrinsic regime. Thus, by setting the valence band edge as zero ($E_v = 0$) we can re-express E_{int} in terms of the energy band gap

$$E_f^{int} = E_c - \frac{E_g(T)}{2} + \frac{3}{4}k_B T \ln\left(\frac{m_p^*}{m_n^*}\right). \quad (18)$$

To reproduce the experimental results of thermoelectric transport properties (S, σ, κ_c) for our p-type samples, it is found to be useful to define the temperature dependence of energy band gap as

$$E_g(T) = \left[E_g(0) - \frac{\alpha T^2}{\beta + T}\right] + \frac{\eta T}{\beta + T}, \quad (19)$$

where $E_g(0)$ is the value of E_g at 0 K, α, β, and η are treated as adjustable parameters and given in Table I. In Eq. (19), the temperature variation of E_g is slightly different from Varshni's expression[35] with the addition of an extra term. The small value of $E_g(0)$, given in Table I, is obtained by considering that the band gap of the $(Bi_2Te_3)_x$ $(Sb_2Te_3)_{1-x}$ alloy shows strong bowing with the indirect band gaps of Bi_2Te_3 and Sb_2Te_3 taken as 0.13 eV and 0.15 eV, respectively.[36] Due to the very narrow band gap of our p-type material we consider the same values of $E_g(0)$ and E_a for all the six samples. To reproduce the experimental measurements of S and σ successfully we found it necessary to include the $E_g(T)$ dependence beyond a critical temperature where the material turns from extrinsic to intrinsic for all the samples. From our work the critical turn-over temperatures (T_c) are 420 K for $x = 0.18$, 0.19, and 0.20; 410 K for $x = 0.22$; 380 K for $x = 0.24$; and 360 K for $x = 0.26$. As clearly seen in Fig. 1, T_c shifts to lower temperatures with increasing the Bi_2Te_3 content in our p-type alloy. This is happening mainly because of the reduction in N_a (in other words the m_p^*/m_n^* ratio) while the x value is increasing. As stated in the experimental works already,[18,22] the electronegativity difference between the Bi and Te atoms is bigger than that between the Sb and Te atoms. Therefore, increasing the Bi_2Te_3 content in $(Bi_2Te_3)_x(Sb_2Te_3)_{1-x}$ single crystals causes lower antistructure defects and results in smaller hole concentration.

As expected for p-type semiconductor materials, positive values of the Seebeck coefficient are calculated theoretically for all the compositions in the range $0.18 \leq x \leq 0.26$ and demonstrated in Fig. 2. The experimental measurements of S values for all the samples worked by Li *et al.*[22] are successfully reproduced throughout the temperature range studied in this work. The temperature dependence of the Seebeck coefficient for all the compositions is found to be similar: it first increases linearly, and after reaching the extrinsic-intrinsic turn-over it decreases with temperature. As can be anticipated from the theoretical calculation of E_f, while the value of x becomes higher, the peak value of S moves to lower temperature due to the reduction in N_a (or the m_p^*/m_n^* ratio). Moreover, from Eq. (4) it is seen that the Seebeck coefficient (S) directly depends on the Fermi level (E_f) and the scattering parameter (r). As illustrated in Fig. 2, in the extrinsic regime the magnitude of S becomes larger with increasing the x value. On the other hand, in the intrinsic regime this is not true for the samples with the compositions $x = 0.22$, 0.24, and 0.26 where the effect of inverse proportionality of r with S becomes dominant. Eventually the maximum value of S is gained for $x = 0.26$ as $S = 236.2\ \mu$V/K at 360 K and the minimum value for S is obtained as 175 μV/K at 290 K for $x = 0.18$.

The theoretical calculation of the electrical resistivity for various x values is presented in Fig. 3, and the experimental results from[22] are included for comparison. In the extrinsic regime we assume theoretically that the most dominant scattering mechanism is caused by the acoustic

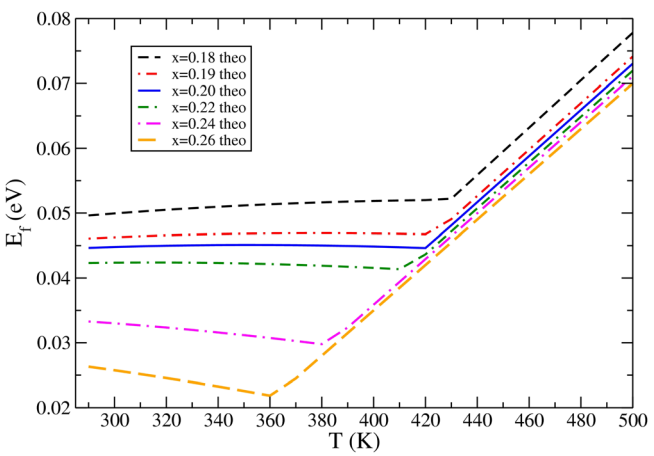

FIG. 1. Temperature dependence of the Fermi level for p-type $(Bi_2Te_3)_x(Sb_2Te_3)_{1-x}$ single crystals doped with 3 wt. % Te.

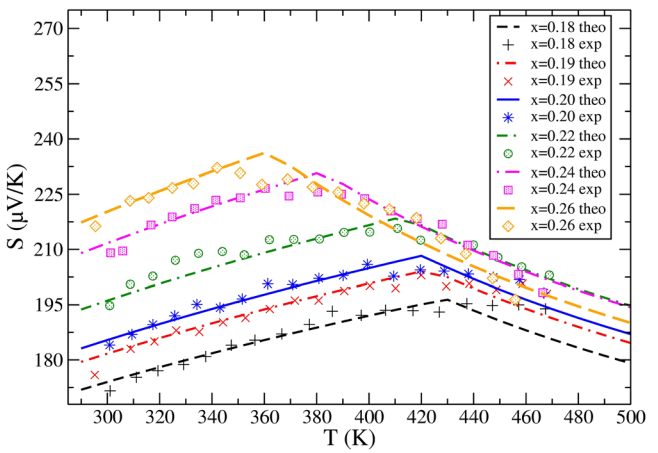

FIG. 2. Temperature dependence of the Seebeck coefficient for p-type $(Bi_2Te_3)_x(Sb_2Te_3)_{1-x}$ single crystals doped with 3 wt. % Te. The symbols represent the experimental measurements read from Li *et al.*[22]

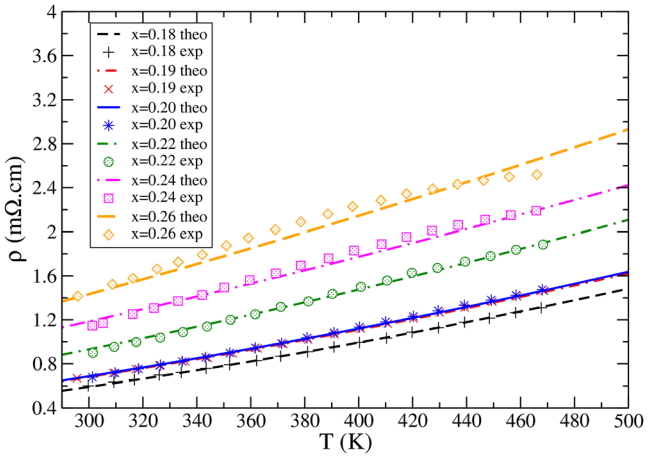

FIG. 3. Temperature dependence of the electrical resistivity for p-type $(Bi_2Te_3)_x(Sb_2Te_3)_{1-x}$ single crystals doped with 3 wt. % Te. The symbols represent the experimental measurements read from Li *et al.*[22]

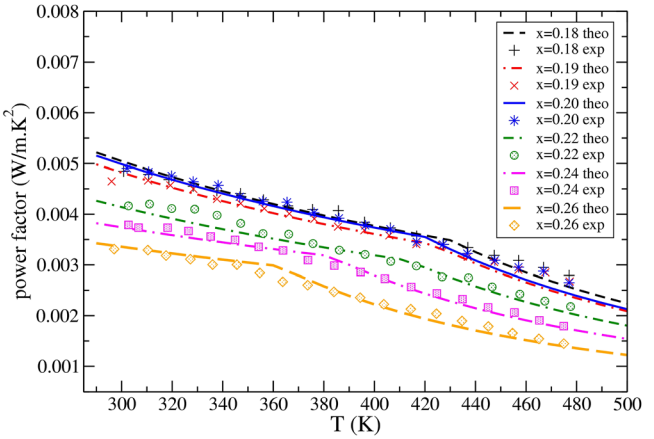

FIG. 4. Temperature dependence of the power factor for p-type $(Bi_2Te_3)_x(Sb_2Te_3)_{1-x}$ single crystals doped with 3 wt. % Te. The symbols represent the experimental results read from Li *et al.*[22]

phonons. In fact, a number of other scattering mechanisms also contribute, e.g., due to optical phonons, impurities, and carrier-carrier. To cover these additional scattering mechanisms and to get an accurate explanation of the experimental measurements we scaled the resistivity ρ in the following form:

$$\rho_{\text{extrinsic}} = \rho_{\text{ext}} A T^{\varsigma}, \tag{20}$$

where A and ς are treated as adjustable parameters as in our previous work[23] and are given in Table I. In the intrinsic regime, additional to Eq. (9) we found that it is necessary to add a temperature dependence of free carrier-phonon scattering to get adequate explanation of the experimental results.[23,37] Thus, the intrinsic electrical resistivity-T dependence can be written as

$$\rho_{\text{intrinsic}} = \rho_{\text{int}} + BT, \tag{21}$$

where B is the temperature independent parameter[23,37] and given in Table I. Using the final expressions for $\rho_{\text{extrinsic}}$ and $\rho_{\text{intrinsic}}$ we successfully explain the experimental measurements of the electrical resistivities for all the compositions as shown in Fig. 3. Throughout the temperature range studied here, the magnitude of the electrical resistivity goes up with increasing the value of x. This results from the rising m_p^* value in the extrinsic regime and increasing the value of B parameter in the intrinsic regime. The lowest value of ρ is attained for the $x = 0.20$ sample for the whole temperature range. It is interesting to note that from the theoretical calculation of the resistivity we did not find any clean signature of the extrinsic-intrinsic turn-over point as in the calculation of E_f and S.

The theoretical calculation of the power factor (PF)-T dependence for all the six compositions is presented in Fig. 4. Based on our accurate theoretical calculation of S and ρ, we successfully reproduce the experimentally expected values of PF for all the six samples.[22] Although the sample with $x = 0.18$ has the lowest value of S among all the compositions, it has the largest value of PF $= 5.21 \times 10^{-3}$ W/(m K^2) near room temperature both theoretically and experimentally. The reason for this is that the power factor is controlled strongly by σ rather than S. It also should be noted that the largest PF value for an n-type $Bi_2(Te_{0.85}Se_{0.15})_3$ single crystal doped with 0.1 wt. % CuBr was obtained as 3.0×10^{-3} W/(m K^2)at 550 K[23] which is nearly half of that for the p-type $x = 0.18$ sample studied here. Furthermore, it is clearly shown in Fig. 4 that the extrinsic-intrinsic turn-over temperatures in PF calculations are the same for all samples as in the E_f and S calculations.

B. Thermal transport coefficients

By employing the Wiedemann-Franz law as described in the theory section, the theoretical calculation of the carrier thermal conductivities (arising from holes) of all the samples are shown in Fig. 5 along with the experimental results reported in Ref. 22. As explained in Eqs. (10) and (11), for our p-type doped Bi_2Te_3 based materials we use the modified and temperature dependent Lorenz number. The value of the $\mathcal{L}$ for the $x = 0.20$ sample is found to be 2.1×10^{-8} W Ω K^{-2}, 2.06×10^{-8} W Ω K^{-2}, and 1.8×10^{-8} W Ω K^{-2} at 300 K, 400 K, and 500 K, respectively. This shows that our modified $\mathcal{L}$ decreases with temperature, and it is smaller than the

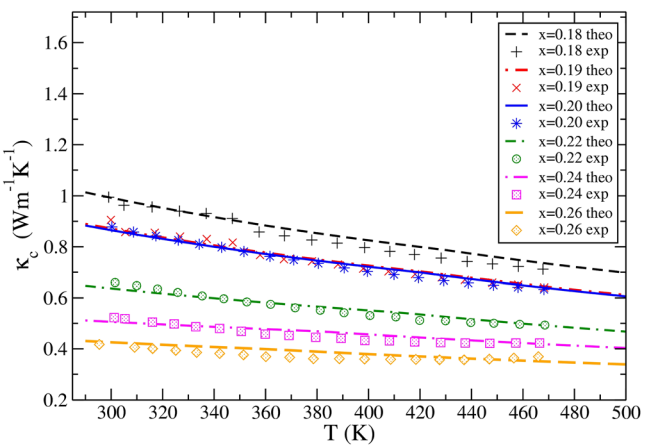

FIG. 5. Temperature dependence of the electronic thermal conductivity for p-type $(Bi_2Te_3)_x$ $(Sb_2Te_3)_{1-x}$ single crystals doped with 3 wt. % Te. The symbols represent the experimental results read from Li *et al.*[22]

Sommerfeld value 2.44×10^{-8} W Ω K^{-2} for metals.[31] The temperature variation of κ_c can be easily understood from the theoretical calculation of ρ. Increasing the Bi_2Te_3 content in our p-type sample leads to smaller values of κ_c throughout the temperature range. As seen in Fig. 5 we successfully reproduce the experimental results of κ_c for all the compositions and find the lowest value of 0.323 W K^{-1} m^{-1} at 500 K for the composition $x = 0.26$.

The theoretical calculation of the $(\kappa_{ph} + \kappa_{bp})$-$T$ variation is presented in Fig. 6 along with the expected experimental values taken from.[22] Using the related parameters given in Table I, the κ_{ph} calculation is made in terms of a temperature independent adjustable parameter $F_{3ph} = (\gamma/\bar{c})^2$. From our theoretical calculations, we note that for all the samples, boundary and hole-phonon scatterings play a major role at low temperatures (below 100 K), and mass-defect scatterings are important at both low and high temperatures (below and above 100 K). Besides this three-phonon interactions become dominant only at high temperatures (above 100 K) for all the six compositions. Additional to these dependences, the bipolar contribution of thermal conductivity (κ_{bp}) is computed theoretically with F_{bp} and p parameters in the range of 290 K and 500 K. As we pointed out already in our previous works,[23,34] κ_{bp} becomes significant when $T > 300$ K for narrow band gap semiconductors. From the parameters $\Gamma_{isotopes}$ and Γ_{alloy} given in Table I, our theoretical calculations suggest that for all the six samples the mass defect-phonon scattering caused by the alloying effect is larger than the isotopic mass defect scattering. Also these $\Gamma_{isotopes}$ and Γ_{alloy} parameters become smaller with increasing the Bi_2Te_3 content in our p-type materials. Moreover, by using more Bi_2Te_3 content, it is seen that the effect of bipolar contribution on thermal conductivity becomes larger. In the temperature range from 290 K to 500 K, $\kappa_{ph} + \kappa_{bp}$ exhibits an almost exponential rise for all the samples, suggesting the electron-hole pair contribution in this temperature range becomes significantly larger compared with other contributions. As seen from the measurements in Ref. 22, samples with $x = 0.18$ and $x = 0.20$ have the lowest values of $\kappa_{ph} + \kappa_{bp}$ among all the samples throughout the temperature range. Our theoretical calculations also support that with higher values of $\Gamma_{isotopes}$ and Γ_{alloy} parameters and lower F_{bp} parameter, smaller $\kappa_{ph} + \kappa_{bp}$ values are found to be 0.375 W m^{-1} K^{-1} for $x = 0.18$ sample and 0.385 W m^{-1} K^{-1} for $x = 0.20$ sample at 330 K.

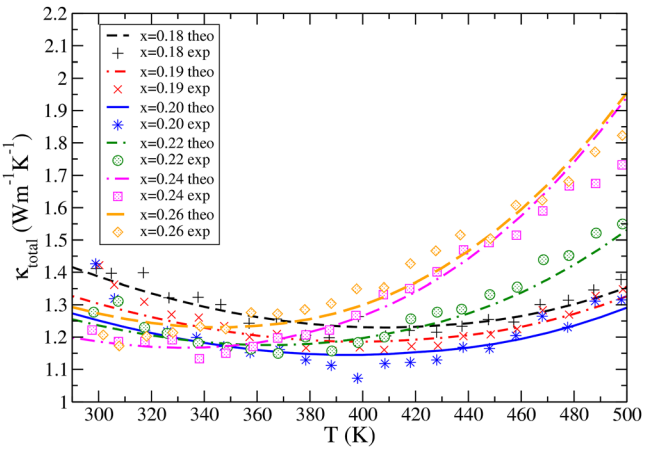

FIG. 7. Temperature dependence of the total thermal conductivity for p-type $(Bi_2Te_3)_x(Sb_2Te_3)_{1-x}$ single crystals doped with 3 wt. % Te. The symbols represent the experimental measurements read from Li *et al.*[22]

The total thermal conductivity is calculated by combining all contribution as $\kappa_{total} = \kappa_c + \kappa_{ph} + \kappa_{bp}$ and presented in Fig. 7 along with the experimental measurements given by Li *et al.*[22] As we expect from our κ_c and $\kappa_{ph} + \kappa_{bp}$ calculations, the magnitude and temperature dependence of κ_{total} for all the samples is analysed accurately. By having one of the lowest $\kappa_{ph} + \kappa_{bp}$ value for the sample with the $x = 0.20$ composition we achieve the smallest κ_{total} value of 1.145 W K^{-1} m^{-1} at 400 K theoretically. This small κ_{total} result will have an important effect in achieving the highest value of ZT for this p-type material. For the comparison of n- and p-type materials, we note $\kappa_{total} = 3.15$ W K^{-1} m^{-1} for n-type $Bi_2(Te_{0.85}Se_{0.15})_3$ single crystal doped with 0.1 wt. % CuBr at 380 K which is three times larger than the result for the $x = 0.20$ p-type material studied here. This comparison

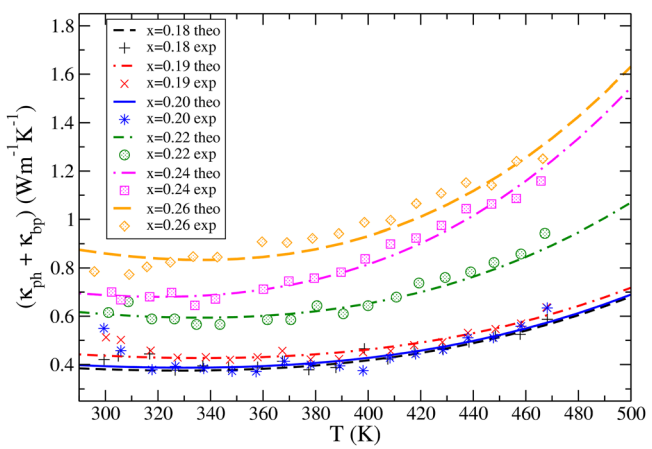

FIG. 6. Temperature dependence of the sum of the lattice and bipolar contributions of thermal conductivity for p-type $(Bi_2Te_3)_x(Sb_2Te_3)_{1-x}$ single crystals doped with 3 wt. % Te. The symbols represent the experimentally expected results read from Li *et al.*[22]

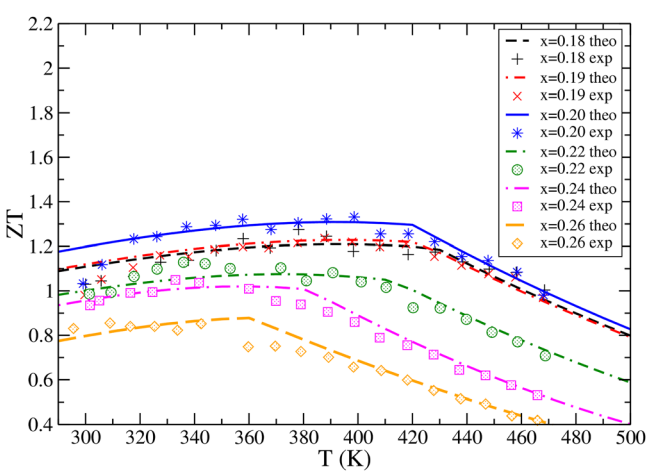

FIG. 8. Temperature dependence of the thermoelectric figure of merit for p-type $(Bi_2Te_3)_x(Sb_2Te_3)_{1-x}$ single crystals doped with 3 wt. % Te. The symbols represent the experimental results read from Li *et al.*[22]

clearly suggests that using p-type Bi_2Te_3 based alloys rather than n-type alloys will produce significantly smaller values of κ_{total}.

C. Thermoelectric figure of merit

We theoretically compute the *ZT* using Eq. (1) for all compositions in the range of $0.18 \leq x \leq 0.26$ and successfully explain the experimental results shown in Fig. 8. For all samples, the temperature dependence of *ZT* is similar: in the extrinsic regime it increases slightly, and after the extrinsic-intrinsic turn-over point it decreases gently. The highest *ZT* value is experimentally obtained for the 20% Bi_2Te_3 - 80% Sb_2Te_3 sample as 1.33 at 398 K. We theoretically find that the $x = 0.20$ sample has the largest *ZT* as 1.31 at 390 K which is in very good agreement with the experimental study.[22] The reason that the $x = 0.20$ sample has the biggest value of *ZT* among the six compositions is twofold: it has the lowest total thermal conductivity and has one of the highest power factor values where the peak value of *ZT* occurs. Additionally, as seen in Fig. 8, when we use less amount of Bi_2Te_3 in our p-type material the effective usage temperature range, with almost a constant *ZT* value, becomes broader. For instance, while a constant *ZT* value is obtained for the $x = 0.26$ sample in the temperature range of $300\,K \leq T \leq 380\,K$, for the $x = 0.20$ sample it is in temperature range $320\,K \leq T \leq 440\,K$.

In Fig. 9 we compare both theoretical and experimental values of *ZT* for the p-type $(Bi_2Te_3)_{0.20}(Sb_2Te_3)_{0.80}$ single crystal doped with 3 wt. % Te studied in the present work and the n-type $Bi_2(Te_{0.85}Se_{0.15})_3$ single crystal doped with 0.1 wt. % CuBr reported in our previous study.[23] As clearly seen *ZT* can be enhanced up to a factor of 2.6 by choosing the p-type material rather than the n-type material. This is due to the larger value of PF and smaller value of κ_{total} for the p-type material. We also note that in the range $300\,K \leq T \leq 500\,K$ the temperature variation of *ZT* is different for n- and p-type alloys: while it monotonously increases for n-type material, after a slight rise it decreases beyond 420 K for p-type material.

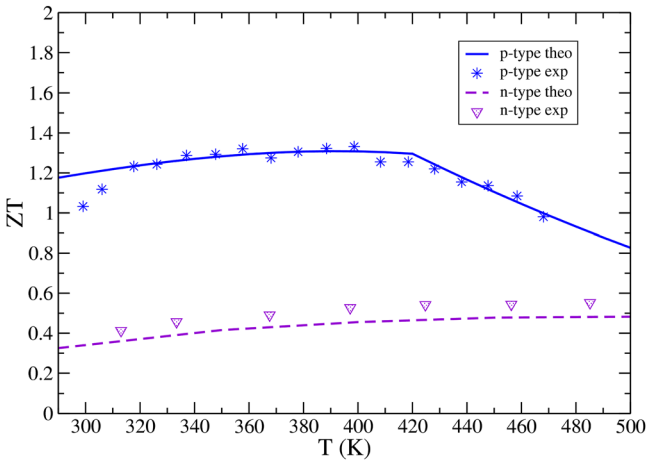

FIG. 9. Temperature dependence of the thermoelectric figure of merit for p-type $(Bi_2Te_3)_x(Sb_2Te_3)_{1-x}$ single crystals doped with 3 wt. % Te and n-type $Bi_2(Te_{0.85}Se_{0.15})_3$ single crystal doped with 0.1 wt. % CuBr studied in Ref. 23. Stars represent the experimental results for the p-type material[22] and triangles show the experimental results for the n-type material studied by Hyun *et al.*[41]

IV. SUMMARY

The purpose of this research was to investigate the thermoelectric properties of p-type $(Bi_2Te_3)_x(Sb_2Te_3)_{1-x}$ single crystal doped with 3 wt. % Te in the composition range $0.18 \leq x \leq 0.26$ and to compare the theoretical calculations with the experimental work studied by Li *et al.*[22] We conclude the following:

(i) For all the compositions, the Fermi level (E_f) first shows an extrinsic semiconductor behaviour, and after an extrinsic-intrinsic turn-over temperature (T_c) it behaves like an intrinsic semiconductor. Also, while the value of *x* increases, T_c shifts to lower temperatures due to decrement in N_a, or equivalently the m_p/m_n ratio.

(ii) The Seebeck coefficient of all samples reflects the temperature variation of E_f. Generally, a larger Bi_2Te_3 content in the p-type material leads to a higher value of *S*. The largest value of *S* is found to be 236.2 μV/K for the $x = 0.26$ sample at 360 K.

(iii) The electrical resistivity of none of the samples shows the extrinsic-intrinsic turn-over points both theoretically and experimentally. The value of ρ increases while the *x* values become larger. This is because of bigger m_p^* values in the extrinsic regime and the larger *B* parameter in the intrinsic regime.

(iv) The smallest amount of Bi_2Te_3 content ($x = 0.18$ sample) in the p-type alloy produces the highest PF of 5.21×10^{-3} W/(m K^2) near 290 K theoretically, which is almost double of that for the n-type $Bi_2(Te_{0.85}Se_{0.15})_3$ single crystal doped with 0.1 wt. % CuBr studied in our previous work.[23]

(v) Higher Bi_2Te_3 content produces lower values of the hole contribution to thermal conductivity (κ_c).

(vi) By applying Srivastava's scheme for phonon conductivity (κ_{ph}) and Price's theory for bipolar contribution (κ_{bp}), reasonable agreement is achieved with the experimental results for all the samples.

(vii) The minimum value of κ_{total} is found to be 1.145 W K^{-1} m^{-1} for the $x = 0.20$ sample at 400 K, which is nearly three times smaller than that for the n-type of material reported previously.[23]

(viii) The experimentally measured *ZT*-T variation for all the samples[22] has been successfully reproduced. The maximum value of *ZT* is computed theoretically as 1.31 for the $x = 0.20$ sample at 390 K, which is determined by the lowest total thermal conductivity and one of the highest power factor values among all compositions. The *ZT* of the p-type $x = 0.20$ sample is 2.6 times larger than that for the n-type sample studied in our previous work.[23] This clearly shows that the influence of the composition range of semiconductor alloys together with its type and amount of dopant plays an important role in enhancing the thermoelectric figure of merit.

ACKNOWLEDGMENTS

Övgü Ceyda Yelgel is grateful for financial support from The Republic of Turkey Ministry of National Education through the Recep Tayyip Erdoğan University in Rize/Turkey (Recep Tayyip Erdoğan Üniversitesi Rektörlüğü, Fener Mah. Merkez Kampüs 53100/RİZE/TÜRKİYE).

[1]D. M. Rowe, *Thermoelectrics Handbook* (Taylor and Francis Group, London, 2006).
[2]T. M. Tritt, *Recent Trends in Thermoelectric Materials Research I* (Academic, San Diego, 2001).
[3]H. J. Goldsmid, *Introduction to Thermoelectricity* (Springer, Berlin, 2010).
[4]R. R. Heikes and R. W. Ure, *Thermoelectricity, Science and Engineering* (Interscience, New York, 1961).
[5]A. F. Ioffe, *Semiconductor Thermoelements and Thermoelectric Cooling* (Infosearch Ltd., London, 1957).
[6]J.-C. Zheng, Fron. Phys. China **3**, 269 (2008).
[7]Y. Lan, A. J. Minnich, G. Chen, and Z. Ren, Adv. Funct. Mater. **20**, 357 (2010).
[8]J. R. Sootsman, D. Y. Chung, and M. G. Kanatzidis, Angew. Chem., Int. Ed. **48**, 8616 (2009).
[9]L. D. Hicks and M. S. Dresselhaus, Phys. Rev. B **47**, 12727 (1993).
[10]X. Sun, Z. Zhang, and M. S. Dresselhaus, Appl. Phys. Lett. **74**, 4005 (1999).
[11]L. D. Hicks, T. C. Harman, X. Sun, and M. S. Dresselhaus, Phys. Rev. B **53**, R10493 (1996).
[12]R. Venkatasubramanian, E. Siivola, T. Colpitts, and O. Quinn, Nature (London) **413**, 597 (2001).
[13]B. Poudel, Q. Hao, Y. Ma, Y. Lan, A. Minnich, B. Yu, X. Yan, D. Wang, A. Muto, D. Vashaee, X. Chen, J. Liu, M. S. Dresselhaus, G. Chen, and Z. Ren, Science **320**, 634 (2008).
[14]V. Goyal, D. Teweldebrhan, and A. Balandin, App. Phys. Lett. **97**, 133117 (2010).
[15]F. Zahid and R. Lake, Appl. Phys. Lett. **97**, 212102 (2010).
[16]T. C. Harman, M. P. Walsh, B. E. Laforge, and G. W. Turner, J. Electron. Mater. **34**, L19 (2005).
[17]G. J. Snyder and E. S. Toberer, Nature Mater. **7**, 105 (2008).
[18]J. Jiang, L. D. Chen, Q. Yao, S. Q. Bai, and Q. Wang, Mater. Chem. Phys. **92**, 39 (2005).
[19]F. Köng, Cryst. Res. Technol. **33**, 219 (1998).
[20]A. L. Bassi, A. Bailini, C. S. Casari, F. Donati, A. Mantegazza, M. Passoni, V. Russo, and C. E. Bottani, J. Appl. Phys. **105**, 124307 (2009).
[21]Y. M. Lin, O. Rabin, S. B. Cronin, J. Y. Ying, and M. S. Dresselhaus, Appl. Phys. Lett. **81**, 2403 (2002).
[22]D. Li, R. R. Sun, and X. Y. Qin, Intermetallics **19**, 2002 (2011).
[23]Ö. C. Yelgel and G. P. Srivastava, Phys. Rev. B **85**, 125207 (2012).
[24]G. P. Srivastava, *The Physics of Phonons* (Taylor and Francis Group, New York, 1990).
[25]P. J. Price, Philos. Mag. **46**, 1252 (1955).
[26]J. P. McKelvey, *Solid State and Semiconductor Physics* (Harper and Row, New York, 1966).
[27]D. M. Rowe and C. M. Bhandari, *Modern Thermoelectrics* (Reston Publishing Company, Virginia, 1983).
[28]B. R. Nag, *Theory of Electrical Transport in Semiconductors* (Pergamon, Oxford, 1972).
[29]A. H. Wilson, *The Theory of Metals* (Cambridge University Press, London, 1953).
[30]C. J. Glassbrenner and G. A. Slack, Phys. Rev. **134**, A1058 (1964).
[31]T. M. Tritt, *Thermal Conductivity Theory, Properties and Applications* (Kluwer Academic/Plenum, London, 2004).
[32]M. G. Holland, Phys. Rev. **134**, A471 (1964).
[33]J. E. Parrott, Rev. Int. Hautes Temp. Refract. **16**, 393 (1979).
[34]Ö. C. Yelgel and G. P. Srivastava, Mater. Res. Soc. Symp. Proc. **1404**, mrsf11-1404-w03-02 (2012).
[35]Y. P. Varshni, Physica **34**, 149 (1967).
[36]N. F. Hinsche, B. Yu. Yavorsky, M. Gradhand, M. Czerner, M. Winkler, J. König, H. Böttner, I. Mertig, and P. Zahn, Phys. Rev. B **86**, 085323 (2012).
[37]C. Kittel, *Introduction to Solid State Physics*, 8th ed. (John Wiley & Sons Inc., USA, 2005).
[38]D. R. Lide, *CRC Handbook of Chemistry and Physics*, 87th ed. (Taylor and Francis Group LLC, 2007).
[39]L. W. Silva and M. Kaviany, Int. J. Heat Mass Transfer **47**, 2417 (2004).
[40]W. Zhang, R. Yu, H. Zhang, X. Dai, and Z. Fang, New J. Phys. **12**, 065013 (2010).
[41]D. B. Hyun, J. S. Hwang, B. C. You, T. S. Oh, and C. W. Hwang, J. Mater. Sci. **33**, 5595 (1998).